

## Supporting Information

### Capacitive deionization in organic solutions: case study using propylene carbonate

S. Porada,<sup>1</sup> G. Feng,<sup>2</sup> M. E. Suss,<sup>3</sup> V. Presser<sup>1,4,\*</sup>

<sup>1</sup> *INM - Leibniz Institute for New Materials, Campus D2 2, 66123 Saarbrücken, Germany*

<sup>2</sup> *State Key Laboratory of Coal Combustion, School of Energy and Power Engineering, Huazhong University of Science and Technology, Wuhan, China*

<sup>3</sup> *Faculty of Mechanical Engineering, Technion - Israel Institute of Technology, Haifa, Israel*

<sup>4</sup> *Department of Materials Science and Engineering, Saarland University, Campus D2 2, 66123 Saarbrücken, Germany*

\* *Corresponding author: volker.presser@leibniz-inm.de*

**Raman spectroscopy.** Raman spectra were measured with a Renishaw inVia Raman Microscope using an Nd-YAG laser with an excitation wavelength of 532 nm. The grating was 2400 lines/mm yielding a spectral resolution of  $\sim 1.2 \text{ cm}^{-1}$  and the spot size on the sample was in the focal plane  $\sim 2 \text{ }\mu\text{m}$  with an output power of 0.2 mW. Spectra were recorded for 20 s and accumulated 50-times to obtain a high signal-to noise and signal-to-background ratio. Peak fitting was performed by employing two Lorentzian peaks, one for the D- and the other for the G-mode.

**Scanning electron microscopy (SEM).** SEM was carried out with a JSM-7500F (JEOL) field-emission system operating at an accelerating voltage of 3 kV. The samples were studied without the application of a conductive sputter coating layer.

**Transmission electron microscopy (TEM).** Samples for transmission electron microscopy (TEM) were prepared by dispersing powders or fibers in ethanol and drop casting them on a copper grid with a lacey carbon film (Gatan). All measurements were carried out with a JEOL 2100F operating at 200 kV.

**Gas sorption analysis (GSA).** To remove adsorbed molecules from the surface, the activated carbon powder was degassed at 200 °C for 30 min and subsequently at 300 °C for 20 h at a relative pressure of 0.1 Pa. Nitrogen gas sorption analysis at -196 °C was performed with a Quantachrome Autosorb 6B system. The pore size distribution (PSD) was derived using the quenched-solid density functional theory (QSDFT) supplied by Quantachrome assuming a slit shape pore model. The specific surface area (SSA) using the BET-equation was calculated in the linear regime of the measured isotherms at a partial pressure range between 0.005 and 0.03  $p/p_0$ .

**Molecular Dynamics (MD) Modeling.** MD simulations were performed in the NPT ensemble using MD package GROMACS.<sup>1</sup> Periodic boundary conditions were used in three dimensions. For organic solution, the force fields for the TEA<sup>+</sup> cations, BF<sub>4</sub><sup>-</sup> anion, and PC molecules were taken from the General Amber Force Field (GAFF),<sup>2</sup> with atomic partial charges from Luzhkov et al.,<sup>3</sup> Wu et al.,<sup>4</sup> and Han et al.<sup>5</sup> For aqueous solution, the force fields for the Na<sup>+</sup> and Cl<sup>-</sup> came from Ref. <sup>6</sup>, and the SPC/E model<sup>7</sup> was used for water molecules. The temperature of all MD systems was maintained at 298 K using the Berendsen thermostat. The electrostatic interactions were computed using the PME method.<sup>8</sup> Specifically, an FFT grid spacing of 0.11 nm and cubic interpolation for charge distribution were used to compute the electrostatic interactions in reciprocal space. A cutoff distance of 1.2 nm and 1.0 nm was used in the calculation of electrostatic interactions in the real space for the organic and aqueous systems, respectively. The non-electrostatic interactions were computed by direct summation with a cutoff length of 1.2 nm and 1.0 nm for the organic and aqueous systems, respectively. The LINCS algorithm<sup>9</sup> was used to maintain the bond lengths within ions/molecules. Each simulation with target ion concentration (i.e., 50 mM and 5 M) was first run for 6 ns to reach equilibrium at 298 K and 1 atm. Then, another 6 ns production run was performed for data analysis. To ensure the statistical accuracy of the simulation results, an ensemble of three MD trajectories with independent initial configurations was utilized.

**Improved Modified Donnan EDL Modeling.** In Fig. 3d, we utilize the improved modified Donnan (i-mD) model to calculate ion concentrations inside micropores from effluent conductivity measurements. The i-mD model used here assumes a symmetric system and uses Eq. 1 (Biesheuvel et al.<sup>10</sup>) assuming that initially there is no charge.

$$c_{\text{ions,mi,initial}} = 2 \cdot c_{\infty,\text{initial}} \cdot \exp(E/c_{\text{ions,mi,initial}}) \quad [1]$$

Where  $c_{\text{ions,mi,initial}}$  is the initial micropore ion concentration ( $c_{\text{ions,mi,initial}} = c_{\text{anion,mi,initial}} + c_{\text{cation,mi,initial}}$ ), which is the concentration in the pores when at equilibrium with the initial electrolyte at a salt concentration of  $c_{\infty,\text{initial}}$  (without applied voltage). Here, we use  $E = 200 \text{ kT} \cdot \text{mM}$ , a value close to previously utilized to fit to data for CDI systems.<sup>11</sup> Next, to analyze a batch experiment, the total ion balance in the CDI system which includes the ions in the electrolyte and in the micropores is given by Eq. 2:

$$n_{\text{ions,total}} = 2 \cdot v_{\text{electrolyte}} \cdot c_{\infty,\text{initial}} + m_{\text{electrode}} \cdot v_{\text{mi}} \cdot c_{\text{ions,mi,initial}} \quad [2]$$

where  $v_{\text{electrolyte}}$  is the volume of the electrolyte used in the batch mode process,  $v_{\text{mi}}$  is the specific volume associated with the micropores (here 0.736 mL/g), and  $m_{\text{electrode}}$  is the mass of both electrodes together, when dry. The final ion concentration in the micropores after charging,  $c_{\text{ions,mi}} = c_{\text{anion,mi}} + c_{\text{cation,mi}}$ , can then be calculated from a mass balance applied after the desalination step, using the measured, or calculated final amount of ions in the electrolyte effluent,  $n_{\text{ions,final}}$  (which is calculated from multiplying  $v_{\text{electrolyte}}$  with the measured, final electrolyte, salt concentration, times two), Eq. 3:

$$c_{\text{ions,mi}} = \frac{(n_{\text{ions,total}} - n_{\text{ions,final}})}{m_{\text{total,electrode}} \cdot v_{\text{mi}}} \quad [3]$$

The relationship between  $c_{\text{ions,mi}}$ , and micropore volumetric charge,  $\sigma_{\text{mi}}$  (in  $\text{C}/\text{m}^3$ ) is given by Eq. 4, see Ref. <sup>11</sup>:

$$c_{\text{ions,mi}} = \sqrt{(2 \cdot c_{\infty,\text{final}} \cdot \exp(E/c_{\text{ions,mi}}))^2 + (\sigma_{\text{mi}}/F)^2} \quad [4]$$

The following two equations are used to derive the counterion and co-ion micropore concentration, and these are the definition of  $\sigma_{\text{mi}}$  and the definition of  $c_{\text{ion,mi}}$  (Eq. 5-6):

$$\sigma_{\text{mi}}/F = \sum_i z_i \cdot c_{\text{mi},i} \quad [5]$$

$$c_{\text{ions,mi}} = c_{\text{counterions,mi}} + c_{\text{co-ions,mi}} \quad [6]$$

From Eq. 5-6, we obtain Eq. 7-8;

$$c_{\text{counterions,mi}} = (\sigma_{\text{mi}} + c_{\text{ions,mi}})/2 \quad [7]$$

$$c_{\text{coions,mi}} = (c_{\text{ions,mi}} - \sigma_{\text{mi}})/2 \quad [8]$$

The data points in **Fig. 3D** are obtained using Eq. 7 and 8, where  $c_{\text{ions,mi}}$  is calculated from Eq. 1-3 using the measured value of  $n_{\text{ions,final}}$  from conductivity effluent measurements and our measured calibration curve relating conductivity to ion concentration (**Fig. S2**). For the theory lines in **Fig. 3D**,  $n_{\text{ions,final}}$  or  $(\sigma_{\text{mi}})$  is treated as an unknown, and thus Eq. 1-4 are solved simultaneously to obtain  $n_{\text{ions,final}}$  and  $c_{\text{ions,mi}}$ .

Finally, charge efficiency can be calculated according to Eq. 9:

$$\Lambda = [(c_{\infty,\text{initial}} - c_{\infty,\text{final}}) \cdot v_{\text{electrolyte}}] / (\sigma_{\text{mi}} \cdot v_{\text{mi}} \cdot m_{\text{electrode}} / F) \quad [9]$$

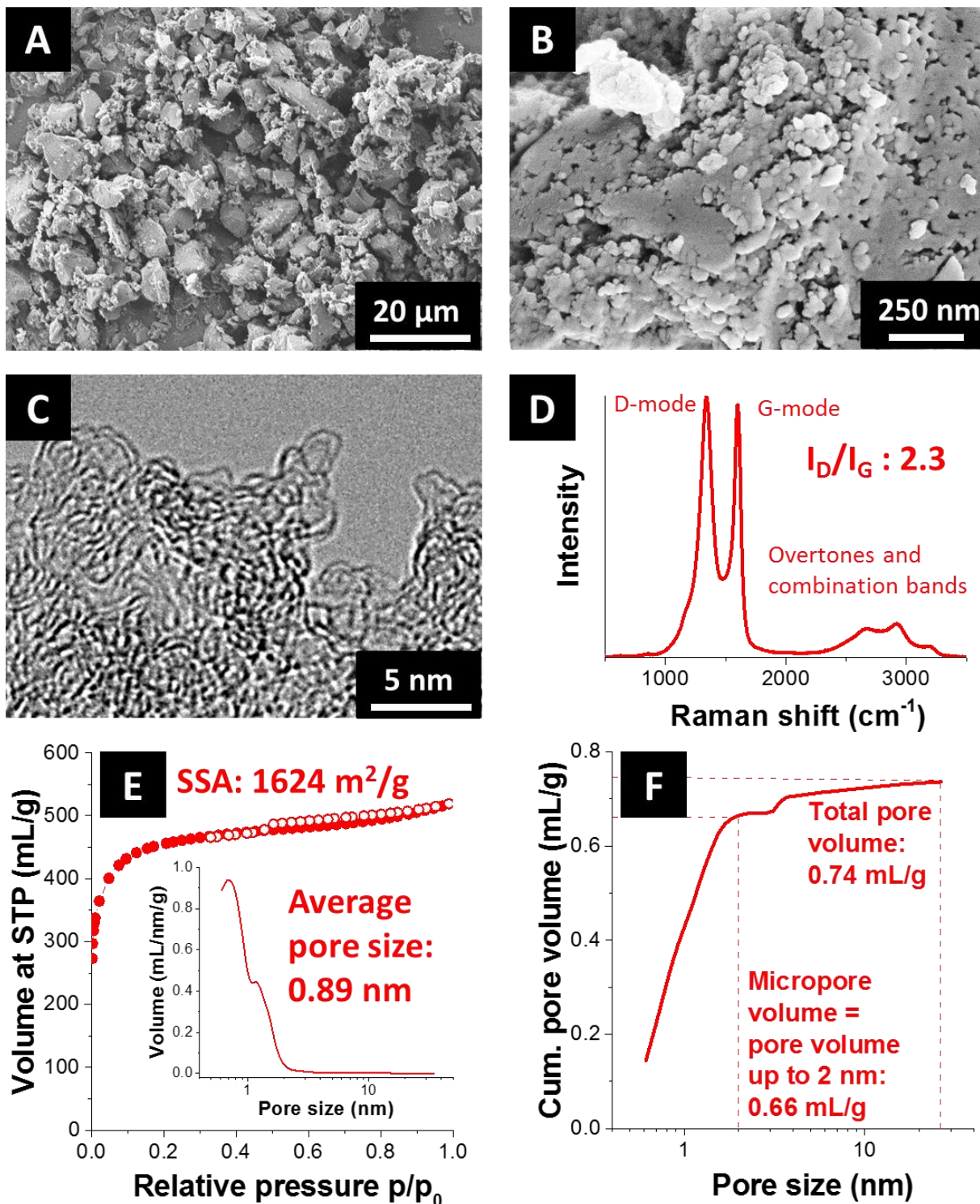


**Fig. S1:** Characterization of YP50-F powder. (A-B) Scanning electron micrographs. (C) Transmission electron micrograph. (D) Raman spectrum recorded at 532 nm. (E) Gas sorption isotherm of nitrogen at -196 °C and calculated pore size distribution (inset) assuming slit-shaped pores and using quenched solid density functional theory (QSDFT) data deconvolution. (F) Cumulative pore size distribution from QSDFT calculations.

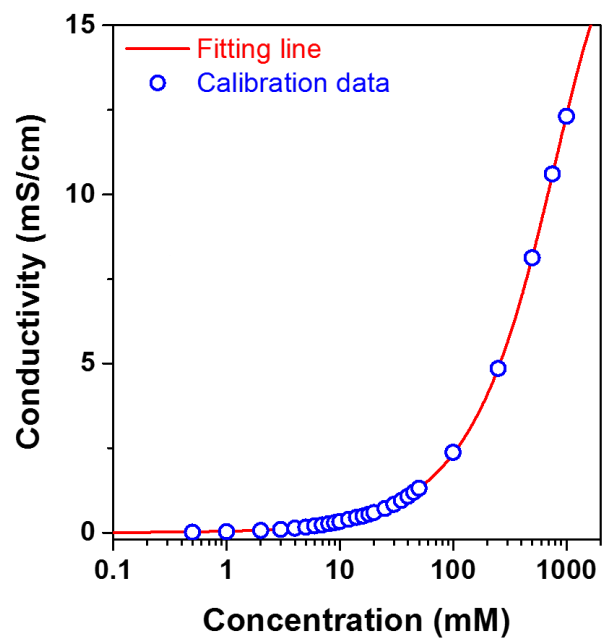


**Fig. S2:** TEA-BF<sub>4</sub> conductivity calibration data in propylene carbonate, PC, over several orders of magnitude of ion concentration.

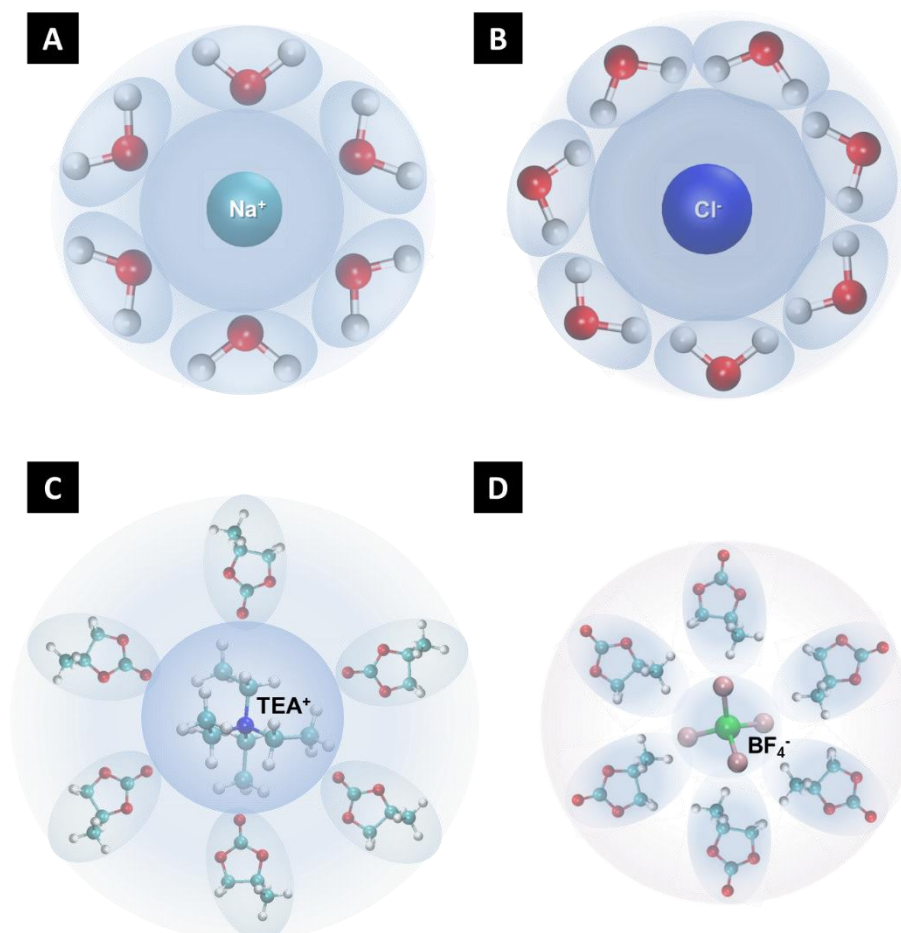


**Fig. S3:** Schematics of solvated ions in 50 mM salt concentration for (A) Na<sup>+</sup> in H<sub>2</sub>O, (B) Cl<sup>-</sup> in H<sub>2</sub>O, (C) TEA<sup>+</sup> in PC, and (D) BF<sub>4</sub><sup>-</sup> in PC. Note that the solvent molecules were drawn here for showing the solvation schematic, and the coordination number of solvent molecules can be found in Table S1.

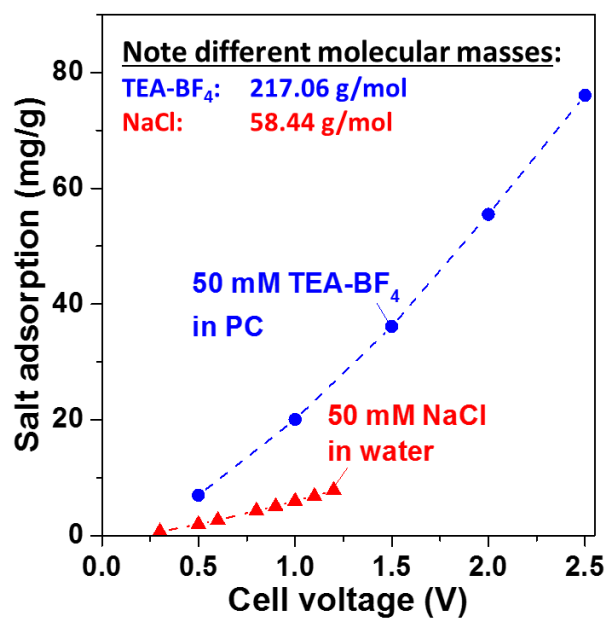


**Fig. S4:** Data presented in Fig. 3B but presented in mg salt per g carbon electrode, not in mmol salt per g carbon electrode.

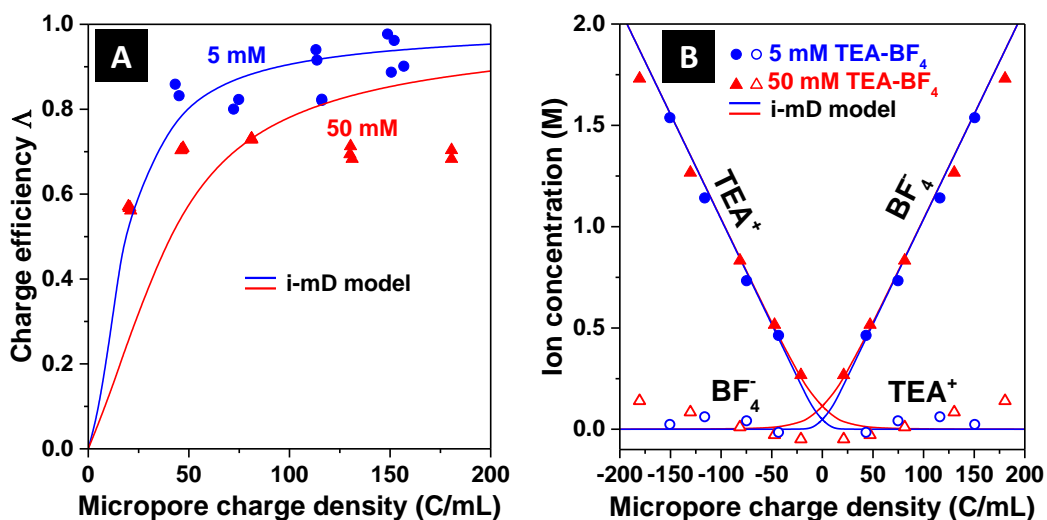


**Fig. S5:** (A) Charge efficiency and (B) ion concentration as function of ionic charge density, and salt concentration,  $c_{\text{salt}}$ , for the CDI system. Solid lines are based on the improved modified Donnan model. These data show that the experimental results for CDI with organic solvents can be well fit using an electrical double-layer (EDL) model developed for micropores, the modified Donnan (i-mD) model (assuming  $E=200 \text{ kT/mM}$  and  $v_{\text{mi}}=0.736 \text{ mL/g}$ ).<sup>10, 11</sup>

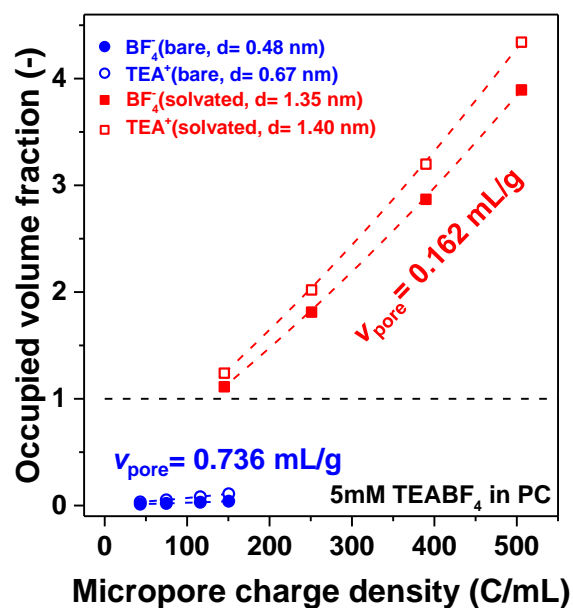


**Fig. S6:** Calculated micropore volume fraction filled with counter-ions, either  $\text{TEA}^+$  or  $\text{BF}_4^-$ , based on corresponding ion sizes and volumes, see Ref. <sup>12-15</sup>. Our analysis was performed assuming (i) total pore volume of 0.736 mL/g available for bare cation, and anion adsorption, (size of a bare cation and anion is equal to 0.67 nm and 0.48 nm respectively),<sup>12</sup> and (ii) a reduced available pore volume of 0.162 mL/g for solvated ions, (solvated cation and anion size is equal to 1.40 nm and 1.35 nm respectively, cut-off value at pore size of 1.35 nm)<sup>14, 15</sup>. See Fig. S1 for porosity data.

**Table S1:** Calculated data on solvated ion sizes and coordination numbers for the aqueous and organic solvent system for NaCl and TEA-BF<sub>4</sub>. Specifically, the solvated ion size corresponds to the first local minimum of the ion-solvent pair correlation function, and the coordinate number is defined as the number of solvent molecules that belong to the solvation shell. The size and coordinate number of solvated Na<sup>+</sup> or Cl<sup>-</sup> are consistent with previous data (Ref. <sup>6</sup>).

| Solvate                      | Solvent          | Concentration (mM) | Solvated ion size (nm) | Coordination number |
|------------------------------|------------------|--------------------|------------------------|---------------------|
| Na <sup>+</sup>              | H <sub>2</sub> O | 50                 | 0.34                   | 6                   |
| Cl <sup>-</sup>              | H <sub>2</sub> O | 50                 | 0.39                   | 7                   |
| Na <sup>+</sup>              | H <sub>2</sub> O | 5                  | 0.34                   | 6                   |
| Cl <sup>-</sup>              | H <sub>2</sub> O | 5                  | 0.39                   | 7                   |
| TEA <sup>+</sup>             | PC               | 50                 | 0.83                   | 16                  |
| BF <sub>4</sub> <sup>-</sup> | PC               | 50                 | 0.67                   | 8                   |
| TEA <sup>+</sup>             | PC               | 5                  | 0.82                   | 16                  |
| BF <sub>4</sub> <sup>-</sup> | PC               | 5                  | 0.67                   | 8                   |

**Table S2:** Calculated diffusion coefficients for Na<sup>+</sup> and Cl<sup>-</sup> in bulk water and TEA<sup>+</sup> and BF<sub>4</sub><sup>-</sup> in bulk propylene carbonate (all data at 1 atm, 24.85 °C, 50 mM), reference values for Na<sup>+</sup> and Cl<sup>-</sup> at infinite dilution are given in brackets (from Ref. <sup>16</sup>).

| Solvate                      | Solvent          | Diffusion coefficient (m <sup>2</sup> /s)        |
|------------------------------|------------------|--|
| Na <sup>+</sup>              | H <sub>2</sub> O | 1.09·10 <sup>-9</sup> , (1.33·10 <sup>-9</sup> ) |
| Cl <sup>-</sup>              | H <sub>2</sub> O | 1.52·10 <sup>-9</sup> , (2.03·10 <sup>-9</sup> ) |
| TEA <sup>+</sup>             | PC               | 3.17·10 <sup>-10</sup>                           |
| BF <sub>4</sub> <sup>-</sup> | PC               | 3.76·10 <sup>-10</sup>                           |

## References

1. E. Lindahl, B. Hess and D. van der Spoel, *J Mol Model*, 2001, **7**, 306-317.
2. J. Wang, R. M. Wolf, J. W. Caldwell, P. A. Kollman and D. A. Case, *J Comput Chem*, 2004, **25**, 1157-1174.
3. V. B. Luzhkov, F. Osterberg, P. Acharya, J. Chattopadhyaya and J. Aqvist, *Physical Chemistry Chemical Physics*, 2002, **4**, 4640-4647.
4. X. Wu, Z. Liu, S. Huang and W. Wang, *Physical Chemistry Chemical Physics*, 2005, **7**, 2771-2779.
5. K. S. Han, N. N. Rajput, X. Wei, W. Wang, J. Z. Hu, K. A. Persson and K. T. Mueller, *The Journal of Chemical Physics*, 2014, **141**, 104509.
6. D. E. Smith and L. X. Dang, *The Journal of Chemical Physics*, 1994, **100**, 3757-3766.
7. H. J. C. Berendsen, J. R. Grigera and T. P. Straatsma, *The Journal of Physical Chemistry*, 1987, **91**, 6269-6271.
8. I.-C. Yeh and M. L. Berkowitz, *The Journal of Chemical Physics*, 1999, **111**, 3155-3162.
9. B. Hess, H. Bekker, H. J. C. Berendsen and J. G. E. M. Fraaije, *J Comput Chem*, 1997, **18**, 1463-1472.
10. P. M. Biesheuvel, S. Porada, M. Levi and M. Z. Bazant, *J Solid State Electr*, 2014, **18**, 1365-1376.
11. T. Kim, J. E. Dykstra, S. Porada, A. van der Wal, J. Yoon and P. M. Biesheuvel, *Journal of Colloid and Interface Science*, 2015, **446**, 317-326.
12. R. Lin, P. L. Taberna, J. Chmiola, D. Guay, Y. Gogotsi and P. Simon, *Journal of The Electrochemical Society*, 2009, **156**, A7-A12.
13. D. H. Aue, H. M. Webb and M. T. Bowers, *Journal of the American Chemical Society*, 1976, **98**, 318-329.
14. Y.-J. Kim, Y. Masuzawa, S. Ozaki, M. Endo and M. S. Dresselhaus, *Journal of the Electrochemical Society*, 2004, **151**, E199-E205.
15. C.-M. Yang, Y.-J. Kim, M. Endo, H. Kanoh, M. Yudasaka, S. Iijima and K. Kaneko, *Journal of the American Chemical Society*, 2006, **129**, 20-21.
16. A. P. Lyubartsev and A. Laaksonen, *The Journal of Physical Chemistry*, 1996, **100**, 16410-16418.